Hindawi
Shock and Vibration
Volume 2017, Article ID 7609528, 11 pages
https://doi.org/10.1155/2017/7609528

*Research Article*

# Dynamical Behavior of a Pseudoelastic Vibration Absorber Using Shape Memory Alloys

**Hugo De S. Oliveira,[1] Aline S. De Paula,[1] and Marcelo A. Savi[2]**

[1]*Department of Mechanical Engineering, Universidade de Brasília, 70910-900 Brasília, DF, Brazil*
[2]*Center for Nonlinear Mechanics, COPPE, Department of Mechanical Engineering, Universidade Federal do Rio de Janeiro, P.O. Box 68.503, 21941-972 Rio de Janeiro, RJ, Brazil*

Correspondence should be addressed to Marcelo A. Savi; savi@mecanica.coppe.ufrj.br

Received 11 April 2017; Accepted 6 July 2017; Published 11 September 2017

Academic Editor: Laurent Mevel



The tuned vibration absorber (TVA) provides vibration reduction of a primary system subjected to external excitation. The idea is to increase the number of system degrees of freedom connecting a secondary system to the primary system. This procedure promotes vibration reduction at its design forcing frequency but two new resonance peaks appear introducing critical behaviors that must be avoided. The use of shape memory alloys (SMAs) can improve the performance of the classical TVA establishing an adaptive TVA (ATVA). This paper deals with the nonlinear dynamics of a passive pseudoelastic tuned vibration absorber with an SMA element. In this regard, a single degree of freedom elastic oscillator is used to represent the primary system, while an extra oscillator with an SMA element represents the secondary system. Temperature dependent behavior of the system allows one to change the system response avoiding undesirable responses. Nevertheless, hysteretic behavior introduces complex characteristics to the system dynamics. The influence of the hysteretic behavior due to stress-induced phase transformation is investigated. The ATVA performance is evaluated by analyzing primary system maximum vibration amplitudes for different forcing amplitudes and frequencies. Numerical simulations establish comparisons of the ATVA results with those obtained from the classical TVA. A parametric study is developed showing the best performance conditions and this information can be useful for design purposes.

## 1. Introduction

Vibration reduction is essential in engineering systems. Critical situations can be related to excessive, undesirable vibrations. Rotor dynamics, robotics, and structural systems are some examples where vibration reduction is essential for a proper and effective performance of the engineering system. The tuned vibration absorber (TVA) is a well-established passive vibration control device for achieving reduction in the vibration of a primary system subjected to external excitation [1]. The TVA consists of a secondary oscillatory system that, once attached to the primary system, is capable of absorbing vibration energy from the primary system. By tuning the natural frequency of the TVA to a chosen excitation frequency, one produces an attenuation of the primary system vibration amplitude for this specific forcing frequency. An alternative for systems where the forcing frequency varies or has a kind of uncertainty is the concept of an adaptive tuned vibration absorber (ATVA). This device is an adaptive-passive vibration control similar to a TVA but with adaptive elements that can be used to change the tuned condition [2, 3].

The remarkable properties of shape memory alloys (SMAs) are attracting technological interest in several science and engineering fields and numerous applications can be imagined including the ones related to applied dynamics. In general, SMAs are being used in order to explore adaptive dissipation associated with hysteresis loop and the mechanical property changes due to phase transformation [4]. Moreover, the dynamical response of systems with SMA actuators presents a unique dynamical behavior due to their intrinsic nonlinear characteristic [4–9]. Another possibility related to SMA dynamical application is its use as constraints exploiting the high dissipation capacity of SMA hysteretic behavior. Hence, SMA can change the system response producing

less complex behaviors when compared with classical elastic constraints [10, 11].

In this regard, SMAs have been used in different ways to perform passive structural vibration control [12, 13]. SMA characteristics motivate the concept of an adaptive tuned vibration absorber that is able to change its stiffness depending on temperature [14–17]. This allows one to attenuate primary system vibration amplitudes not only for one specific forcing frequency, as occurs with the TVA, but also for a broad range of frequencies. In general, the literature discusses the effect of property change due to the temperature-induced phase transformation in SMA-ATVA devices, and there are few reports treating the influence of the hysteretic behavior due to stress-induced phase transformation. Savi et al. [18] presented a discussion about the influence of the hysteretic behavior due to stress-induced phase transformation in pseudoelastic regime of the SMA element of the ATVA. The performance of the pseudoelastic SMA-ATVA for different temperatures was investigated showing vibration reduction in different frequency ranges.

This article revisits the SMA-ATVA considering a parametric analysis with constant temperature. The goal is to identify proper parameters for the system, as the mass ratio between primary system and absorber, and suitable forcing amplitude range where the SMA-ATVA presents better performance than the classical linear TVA. Basically, a secondary system composed of a single degree of freedom oscillator with an SMA element, representing the ATVA, is coupled to a primary system represented by a single degree of freedom linear oscillator. The SMA-ATVA performance is evaluated by analyzing primary system maximum vibration amplitudes for different forcing amplitudes and frequencies. The influence of the hysteretic behavior due to stress-induced phase transformation is considered. A proper constitutive description is employed in order to capture the general thermomechanical aspects of the SMAs. All results from the SMA-ATVA are compared with those obtained from the classical TVA, establishing a proper contrast between the devices and their capacity to promote vibration reduction.

## 2. Constitutive Model

The thermomechanical description of shape memory alloys is the objective of numerous research efforts that try to contemplate all behavior details [19, 20]. Here, a constitutive model proposed by Paiva et al. [21] is employed. This model considers different material properties for each phase and four macroscopic phases, being built upon Fremond's model.

The SMA description considers as main variables the total strain, $\varepsilon$, temperature, $T$, and four internal variables that represent the volume fraction of each macroscopic phase: $\beta_1$ and $\beta_2$, related to detwinned martensites, respectively, associated with tension and compression; $\beta_3$ that represents the volume fraction of austenite; and $\beta_4$ that represents the volume fraction of twinned martensite. Since there is a constraint criterion based on phase coexistence, $\beta_1+\beta_2+\beta_3+\beta_4=1$, it is possible to use only three volume fractions and the thermomechanical behavior of the SMA is described by the following set of equations:

$$\begin{aligned}
\sigma &= E\varepsilon + \left[E\alpha_h + \alpha\right](\beta_2-\beta_1) - \Omega\,(T-T_0)\,,\\
\dot\beta_1 &= \frac{1}{\eta_1}\left\{\alpha\varepsilon + \Lambda_1(T) + \left(2\alpha\alpha_h + E\alpha_h^2\right)(\beta_2-\beta_1)\right.\\
&\quad \left. + \alpha_h\left[E\varepsilon - \Omega\,(T-T_0)\right] - \partial_{\beta_1}J_\pi\right\} + \partial_{\dot\beta_1}J_\chi,\\
\dot\beta_2 &= \frac{1}{\eta_2}\left\{-\alpha\varepsilon + \Lambda_2(T) - \left(2\alpha\alpha_h + E\alpha_h^2\right)(\beta_2-\beta_1)\right.\\
&\quad \left. - \alpha_h\left[E\varepsilon - \Omega\,(T-T_0)\right] - \partial_{\beta_2}J_\pi\right\} + \partial_{\dot\beta_2}J_\chi,\\
\dot\beta_3 &= \frac{1}{\eta_3}\left\{-\frac{1}{2}(E_A-E_M)\left[\varepsilon+\alpha_h(\beta_2-\beta_1)\right]^2 + \Lambda_3(T)\right.\\
&\quad + (\Omega_A-\Omega_M)(T-T_0)\left[\varepsilon+\alpha_h(\beta_2-\beta_1)\right] - \left.\partial_{\beta_3}J_\pi\right\}\\
&\quad + \partial_{\dot\beta_3}J_\chi.
\end{aligned} \tag{1}$$

Here, $\sigma$ is the stress and $E = E_M + \beta_3(E_A - E_M)$ is the elastic modulus, while $\Omega = \Omega_M + \beta_3(\Omega_A - \Omega_M)$ is related to thermal expansion coefficient. Note that subscript $A$ refers to austenitic phase, while $M$ refers to martensite. Parameters $\Lambda_1 = \Lambda_2 = \Lambda = \Lambda(T)$ and $\Lambda_3 = \Lambda_2(T)$ are associated with phase transformation stress levels. Parameter $\alpha_h$ defines the horizontal width of the stress-strain hysteresis loop, while $\alpha$ controls the height of the same hysteresis loop. The terms $\partial_n J_\pi$ ($n = \beta_1, \beta_2, \beta_3$) are subdifferentials of the indicator function $J_\pi$ with respect to $n$. This indicator function is related to a convex set, which provides the internal constraints related to the coexistence of phases. With respect to evolution equations of volume fractions, $\eta_1 = \eta_2 = \eta$ and $\eta_3$ represent the internal dissipation related to phase transformations. Moreover, $\partial_n J_\chi$ ($n = \beta_1, \beta_2, \beta_3$) are subdifferentials of the indicator function $J_\chi$ with respect to $n$. This indicator function is related to the convex set $\chi$, which establishes conditions for the correct description of internal subloops due to incomplete phase transformations. Lagrange multipliers associated with the mentioned constraints may replace these subdifferentials.

Concerning parameter definitions, temperature dependent relations are adopted for $\Lambda$ and $\Lambda_3$ as follows:

$$\begin{aligned}
\Lambda &= \begin{cases} -L_0 + \dfrac{L}{T_M}(T-T_M), & \text{if } T > T_M \\ -L_0, & \text{if } T \le T_M; \end{cases}\\
\Lambda_3 &= \begin{cases} -L_0^A + \dfrac{L^A}{T_M}(T-T_M), & \text{if } T > T_M \\ -L_0^A, & \text{if } T \le T_M. \end{cases}
\end{aligned} \tag{2}$$

Here $T_M$ is the temperature below which the martensitic phase becomes stable. Usually, experimental tests provide information of $M_s$ and $M_f$ and temperatures of the start and finish of the martensitic formation. This model uses only one temperature that could be an average value or alternatively $M_s$ value. Moreover, $L_0$, $L$, $L_0^A$, and $L^A$ are parameters related to critical stress for phase transformation.

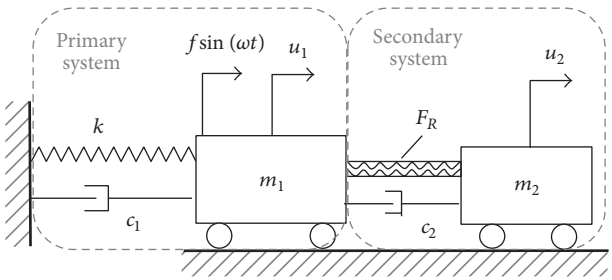


Figure 1: 2DOF SMA oscillator representing the primary system connected to the ATVA (secondary system).

In order to describe the characteristics of phase transformation kinetics, different values of $\eta$ and $\eta_3$ might be considered during loading, $\eta^L$ and $\eta_3^L$, and unloading processes, $\eta^U$, $\eta_3^U$. For more details about the constitutive model, see Paiva et al. [21]. All constitutive parameters can be matched from stress-strain tests.

## 3. Equations of Motion

The SMA-ATVA represents a secondary system that is attached to a primary system, which is represented by a linear oscillator. Therefore, the whole system is a 2DOF oscillator with an SMA element, shown in Figure 1 [18, 22]. The governing equations are obtained from the balance of momentum and it is assumed that the restitution force of the SMA element, $F_R$, is described by the constitutive equations presented in the previous section. Under these assumptions, the equations of motion are given following the same formalism presented in Savi et al. [18]:

$$\begin{aligned} &m_1\ddot{u}_1 + (c_1 + c_2)\dot{u}_1 - c_2\dot{u}_2 + ku_1 \\ &\quad - \frac{EA}{l}(u_2 - u_1) = f\sin(\omega t), \\ &m_2\ddot{u}_2 - c_2\dot{u}_1 + c_2\dot{u}_2 + \frac{EA}{l}(u_2 - u_1) \\ &\quad + (A\alpha + EA\alpha_h)(\beta_2 - \beta_1) - \Omega A(T - T_0) = 0. \end{aligned} \tag{3}$$

In order to establish a nondimensional equation of motion, the following nondimensional parameters are defined:

$$\begin{aligned} \omega_{01}^2 &= \frac{k}{m_1}; \\ \omega_{02}^2 &= \frac{E_R A}{m_2 l}; \\ \xi_1 &= \frac{c_1}{m_1\omega_{02}}; \\ \xi_2 &= \frac{c_2}{m_2\omega_{02}}; \\ \mu_E &= \frac{E}{E_R}; \\ \mu_\Omega &= \frac{\Omega}{\Omega_R}; \\ \gamma_\omega &= \frac{\omega_{01}^2}{\omega_{02}^2}; \\ \gamma_m &= \frac{m_2}{m_1}; \\ \overline{\alpha}_h &= \frac{\alpha_h E_R A}{m_2 l\omega_{02}^2} = \alpha_h; \\ \overline{\alpha} &= \frac{\alpha A}{m_2 l\omega_{02}^2} = \frac{\alpha}{E_R}; \\ \varpi &= \frac{\omega}{\omega_{02}}, \\ \delta &= \frac{f}{m_1 l\omega_{02}^2} = \frac{m_2}{m_1}\frac{f}{E_R A}; \\ \overline{\Omega} &= \frac{\Omega_R A T_R}{m_2 l\omega_{02}^2} = \frac{\Omega_R T_R}{E_R}, \end{aligned} \tag{4}$$

where subscript $R$ is employed to define a reference that can be $M$ (martensite) or $A$ (austenite), for instance. In addition, nondimensional variables associated with displacements $U_1$ and $U_2$, temperature, $\theta$, time, and $\tau$ are defined:

$$\begin{aligned} U_1 &= \frac{u_1}{l}; \\ U_2 &= \frac{u_2}{l}; \\ \theta &= \frac{T}{T_R}; \\ \tau &= \omega_{02} t. \end{aligned} \tag{5}$$

Using these definitions, equations of motion can be rewritten in a nondimensional form as follows [18]:

$$\begin{aligned} &U_1'' + (\xi_1 + \gamma_m\xi_2)U_1' - \gamma_m\xi_2 U_2' + \gamma_\omega U_1 \\ &\quad - \gamma_m\mu_E(U_2 - U_1) = \delta\sin(\varpi\tau), \\ &U_2'' - \xi_2 U_1' + \xi_2 U_2' + \mu_E(U_2 - U_1) \\ &\quad + (\overline{\alpha} + \mu_E\overline{\alpha}_h)(\beta_2 - \beta_1) - \mu_\Omega\overline{\Omega}(\theta - \theta_0) = 0, \end{aligned} \tag{6}$$

where $()' = d()/d\tau$.

The performance of the SMA-ATVA is compared with a classical linear TVA. The 2DOF linear system is similar to the one presented in Figure 1 but replacing the SMA element by an elastic element with stiffness, $k_2 = EA/l$, equivalent to the SMA stiffness at austenitic phase and when phase transformations do not occur [18].

Table 1: SMA parameters.

| | |
|---|---|
| $E_R$ (GPa) | 54 |
| $E_M$ (GPa) | 42 |
| $\alpha$ (MPa) | 330 |
| $\alpha_h$ | 0.048 |
| $L_0$ (MPa) | 0.015 |
| $L$ (MPa) | 41.5 |
| ${L_0}^A$ (MPa) | 0.63 |
| $L^A$ (MPa) | 185 |
| $\Omega_A$ (MPa/K) | 0.74 |
| $\Omega_M$ (MPa/K) | 0.17 |
| $T_M$ (K) | 291.4 |
| $\eta^L$ (MPa·s) | 1.0 |
| $\eta^U$ (MPa·s) | 2.7 |
| $\eta_3^L$ (MPa·s) | 1.0 |
| $\eta_3^U$ (MPa·s) | 2.7 |

## 4. Numerical Simulations

This section presents a numerical investigation of the SMA-ATVA system. In order to deal with nonlinearities of the equations of motion, an iterative procedure based on the operator split technique [23] is employed. Under this assumption, the fourth-order Runge–Kutta method is used together with the projection algorithm to solve the constitutive equations [8, 18]. The solution of the constitutive equations also employs the operator split technique together with an implicit Euler method. The calculation of $\beta_n$ $(n = 1, 2, 3)$ considers that the evolution equations are solved in a decoupled way. Initially, equations are solved (except for the subdifferentials) using an iterative implicit Euler method. If the estimated results obtained for $\beta_n$ do not satisfy the imposed constraints, an orthogonal projection algorithm pulls their value to the nearest point on the domain's surface [5].

Parameters employed in the numerical simulations are presented in Table 1. Besides, simulations are carried out at a temperature of 340 K where only austenitic phase is stable at a stress-free state. The idea to consider a constant temperature is to exploit other parameter variation analyses showing their influence on system dynamics. Savi et al. [18] showed the influence of temperature variation.

The objective of the TVA is the vibration reduction of the primary system, which is under a resonant condition at $\bar{\omega} = 1.135$. However, it must be highlighted that the introduction of TVA usually produces two new shifted resonant peaks that need to be possibly reduced. Hence, the SMA-ATVA behavior is compared with the one presented by the classical TVA, analyzing the response of both systems. The main result is related to maximum amplitude of the primary system and the plots consider steady state behavior. A parametric analysis is carried out, analyzing the performance of both absorbers. Basically, frequency variations are investigated considering different forcing amplitudes and mass ratios. Up-sweep and down-sweep tests are treated considering four distinct situations that describe behavior trends: $\delta = 0.0011$ and $\gamma_m = 0.22$, considered as a reference case; $\delta = 0.0011$ and $\gamma_m = 0.15$, evaluating the influence of mass ratio reduction; $\delta = 0.0025$ and $\gamma_m = 0.22$, evaluating the influence of forcing amplitude increase; $\delta = 0.0025$ and $\gamma_m = 0.10$, evaluating the influence of large amplitudes with small mass ratio.

Initially, the reference case is treated considering forcing amplitude, $\delta = 0.0011$, and mass ratio, $\gamma_m = 0.22$. Forcing frequency is varied considering an up-sweep increase. Figure 2(a) presents steady state maximum amplitude of the 1DOF oscillator and of primary system when the secondary system is attached, considering both SMA-ATVA and TVA. For this mass ratio, a comparison between both absorbers shows that SMA-ATVA promotes a reduction of the primary system vibration around 40% at first resonance peak when compared to the linear classical TVA. In the second resonance region, the maximum amplitudes are similar in both cases and a small dynamical jump occurs with SMA-ATVA attached. Figure 2(b) presents bifurcation diagram, constructed from Poincaré sections, showing that the primary system has periodic responses for all forcing frequencies. Phase space plots together with Poincaré section are presented in Figures 2(c) and 2(d), showing period-1 orbit of the primary system at the first and second resonance frequencies. Figures 2(e) and 2(f) show stress-strain curves for each one of the responses. Note that small amount of phase transformation is occurring, being related to internal subloops.

Figure 3 presents results obtained with down-sweep tests, decreasing the forcing frequency, showing similar behavior of the up-sweep test. Basically, the primary system presents periodic response and a considerable reduction of vibration amplitudes. The main difference is a dynamical jump that occurs close to the first resonance region and a bigger range of forcing frequency related to first resonance region when considering the TVA.

The influence of the mass ratio at this forcing amplitude level is treated by considering the same amplitude of the reference case, $\delta = 0.0011$, but with a smaller mass ratio of $\gamma_m = 0.15$. Figure 4(a) presents steady state maximum amplitude of the 1DOF oscillator and of primary system when the secondary system is attached, considering both SMA-ATVA and TVA. Note that there is a significant reduction of the maximum amplitude at the first resonance region of approximately 25%. For a better understanding of system behavior, Figure 4(b) presents bifurcation diagram of the primary system using the SMA-ATVA. Different from the previous analyzed situation, where a higher mass ratio was considered, a nonperiodic response is observed in the first resonance region. This nonperiodic response can be better analyzed by Figures 4(c) and 4(d) that shows the phase space with Poincaré section for $\bar{\omega} = 0.75$ and $\bar{\omega} = 0.76$, indicating a quasi-periodic response of the system. This behavior is related to stress-induced phase transformations presenting a hysteretic behavior, as shown in Figures 4(f)–4(h). Note that the system follows internal subloops due to incomplete phase transformations. Regarding the second resonance region, the maximum amplitudes of primary system are close to both situations. However, the SMA-ATVA presents a small dynamical jump associated with a transition from a linear response to a nonlinear response related to an incomplete hysteresis loop. Oliveira et al. [9] discussed similar situations related to a 1DOF SMA oscillator. Different from the first

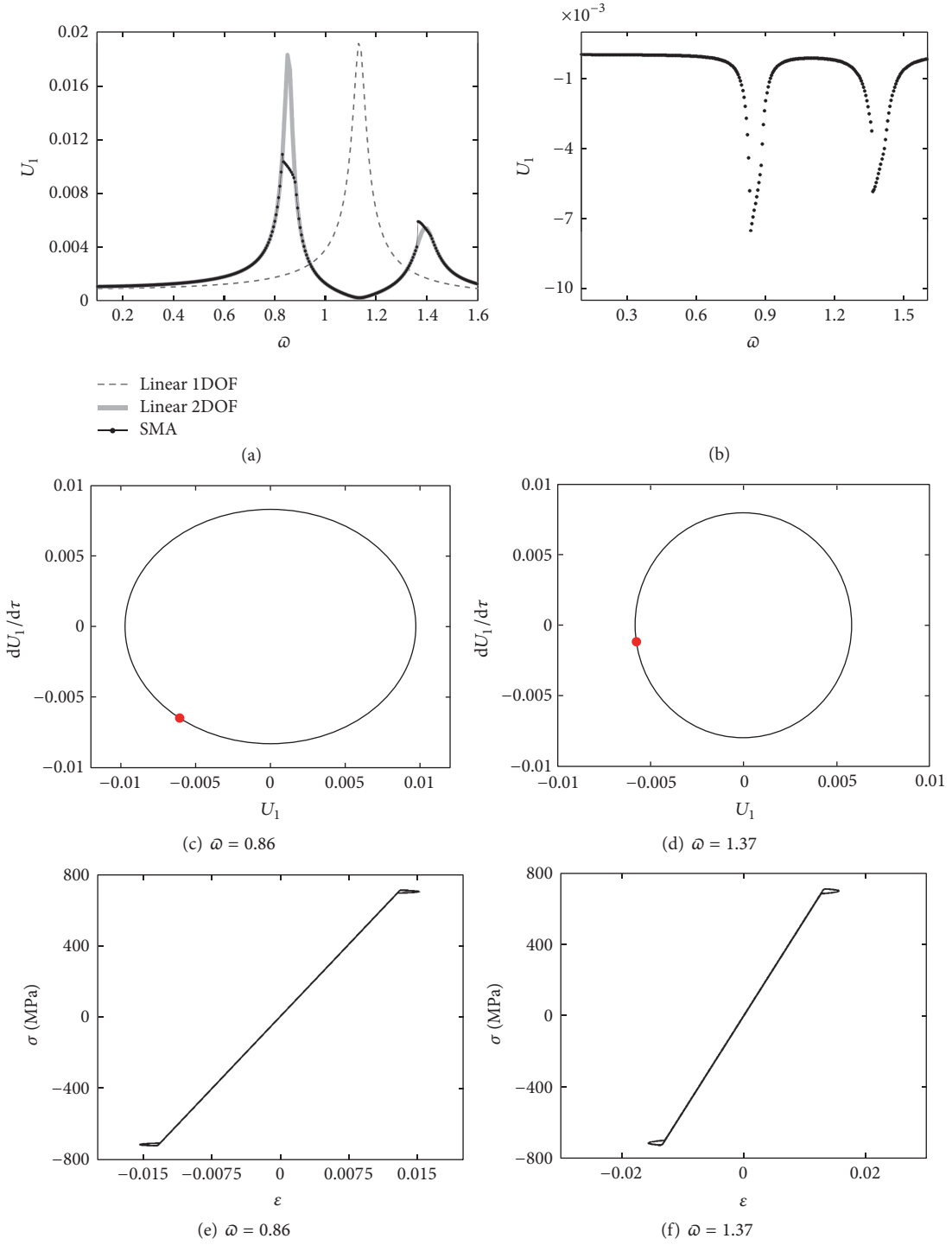


FIGURE 2: Primary system response with $\delta = 0.0011$ and $\gamma_m = 0.22$ in up-sweep test: (a) maximum amplitude; (b) bifurcation diagram; (c-d) phase space with Poincaré section; (e-f) stress-strain diagram.

peak, the second peak is not associated with a nonperiodic behavior, as shown in Figure 4(e), and SMA element presents an incomplete hysteresis loop, as presented in Figure 4(h).

By considering the down-sweep situation, keeping all other parameters constant, SMA-ATVA still presents smaller maximum amplitudes than the TVA responses, Figure 5(a). Moreover, the region related to a nonperiodic response is bigger than the up-sweep case, as it can be observed in bifurcation diagram shown in Figure 5(b). A quasi-periodic like behavior can be identified in the first resonance region as it occurs in the up-sweep case and the SMA element presents incomplete phase transformations following internal hysteretic subloops. In the second resonance region, SMA-ATVA response presents a dynamical jump; however, the

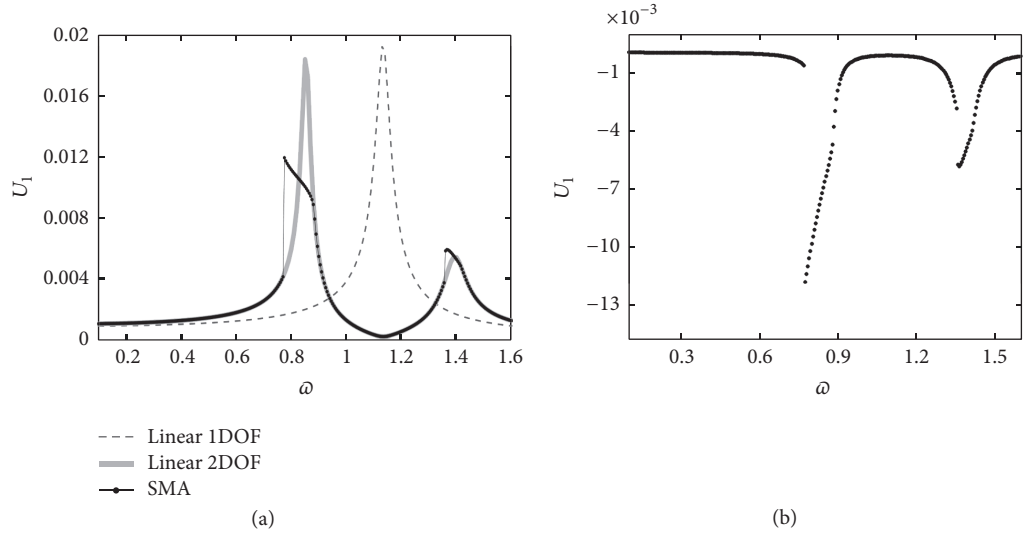


Figure 3: Primary system response with $\delta = 0.0011$ and $\gamma_m = 0.22$ in down-sweep test: (a) maximum amplitude; (b) bifurcation diagram.

primary system maximum amplitude is slightly bigger than the TVA case and occurs in a smaller forcing frequency.

Additional numerical simulations assure that, for the same forcing amplitude of $\delta = 0.0011$, the decrease of mass ratio induces this kind of behavior. When the mass ratio becomes less than or equal to 0.08, the behavior becomes periodic in all range of analyzed forcing frequency, similar to the situation presented in Figures 2 and 3. For this smaller mass ratio, however, SMA-ATVA and TVA present similar performance and, therefore, the use of SMA does not provide any benefit. The limit of this trend is observed when mass ratio is very small (becoming close to zero), situation where the system has a response similar to a single degree of freedom oscillator.

The influence of forcing amplitude is now investigated considering the same mass ratio of the reference case, $\gamma_m = 0.22$, but adopting higher forcing amplitude: $\delta = 0.0025$. Figure 6 presents primary system response by considering an up-sweep increase of the forcing frequency. For this mass ratio, the SMA-ATVA attachment promotes a reduction of the primary system vibration at first resonance peak about 75% when compared to the classical TVA, as shown in Figure 6(a). In the second resonance region, the maximum amplitudes with SMA-ATVA become bigger than the ones related to the TVA and, in addition, a small dynamical jump is observed. It is important to note, however, that the maximum amplitudes in the second resonance region with SMA-ATVA are approximately half of the amplitudes that occur in the first resonance region when considering linear TVA. This situation can be identified as a benefit of the use of SMA-ATVA. From the bifurcation diagram, Figure 6(b), it is noticed that primary system has a periodic response for all forcing frequencies. Figure 7 presents results obtained with down-sweep tests, decreasing the forcing frequency, showing similar behavior of the up-sweep test. Note that this system presents a similar response to the one presented in the first analyzed case (Figures 2 and 3) but with higher amplitudes.

Now, the influence of higher levels of forcing amplitude is evaluated together with small mass ratio and the following parameters are adopted to represent this system: $\delta = 0.0025$ and $\gamma_m = 0.10$. Figure 8 shows primary system behavior for the up-sweep test, by increasing the forcing frequency. Figure 8(a) shows the maximum amplitude of 1DOF and of primary system when the secondary system is attached, considering both SMA-ATVA and TVA. Note that the use of SMA-ATVA presents a huge reduction of vibration of the first resonance peak, around 60%, when compared to the use of linear TVA. Nevertheless, a large region of nonperiodic response is observed in Figure 8(b). Figures 8(c) and 8(d) show details of this nonperiod behavior for $\varpi = 0.63$ and $\varpi = 0.67$, two frequencies inside the first resonance region. In the first frequency, primary system presents a periodic orbit with high periodicity, while the second frequency is related to a chaotic-like response. In both frequencies, the SMA element presents complete phase transformations associated with major hysteresis loop, as shown in Figures 8(e) and 8(f). Regarding the second resonance region, the SMA-ATVA presents a dynamical jump that occurs in a smaller forcing frequency when compared to second resonance peak of the linear system. It should be pointed out that the vibration amplitudes in the second resonance region are considerably small when compared with the first resonance region.

Down-sweep test is presented in Figure 9. Once again, a reduction of the vibration amplitudes is observed in the first resonance region, Figure 9(a), which is related to a nonperiod response, as identified by the bifurcation diagram showed in Figure 9(b). The details of this nonperiodic response are shown with the aid of phase space and Poincaré section presented in Figures 9(c) and 9(d). Stress-strain curves show complete phase transformations related to major hysteresis loops of the SMA element, Figures 9(e) and 9(f). In the second resonance region, primary system with SMA-ATVA presents higher vibration amplitudes when compared to linear TVA. The maximum amplitude of the second resonance region

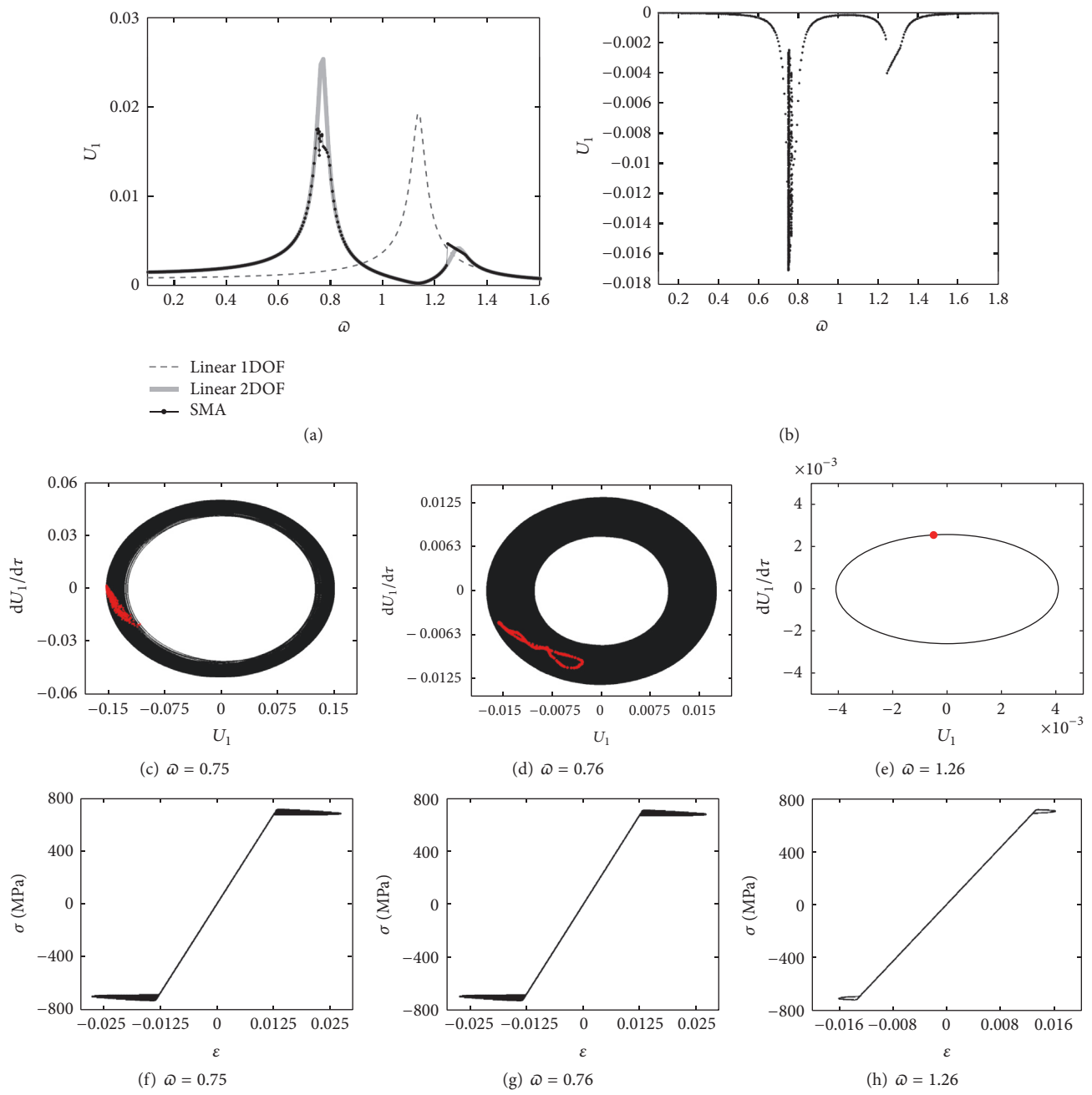


FIGURE 4: Primary system response with $\delta = 0.0011$ and $\gamma_m = 0.15$ in up-sweep test: (a) maximum amplitude; (b) bifurcation diagram; (c–e) phase space with Poincaré section; (f–h) stress-strain curves.

has a similar value of the maximum amplitude of the first resonance region and occurs in a smaller forcing frequency when compared to the second resonance peak of linear system. Basically, it is observed that the use of SMA-ATVA system makes both resonance regions close to each other.

Additional simulations show that, for $\delta = 0.0025$, the reduction of mass ratio from 0.21 to 0.02 promotes a change in system response from a chaotic-like to a periodic pattern. During the transition, a quasi-periodic response is observed, being related to a narrow range of forcing frequency. When the mass ratio is less than or equal to 0.02, the system presents a periodic behavior in all range of analyzed forcing frequency.

The parametric analysis establishes a general tendency that is observed from different simulations. Based on that, it is possible to highlight the main conclusions about the use of SMA-ATVA. For $\delta \leq 0.0025$, the performance of the SMA-ATVA is satisfactory and presents benefits when compared to the classical TVA. When large forcing amplitudes are considered, $\delta > 0.0025$, the SMA-ATVA does not present a satisfactory performance and it leads to more complex responses. In this range of forcing amplitude ($\delta \leq 0.0025$),

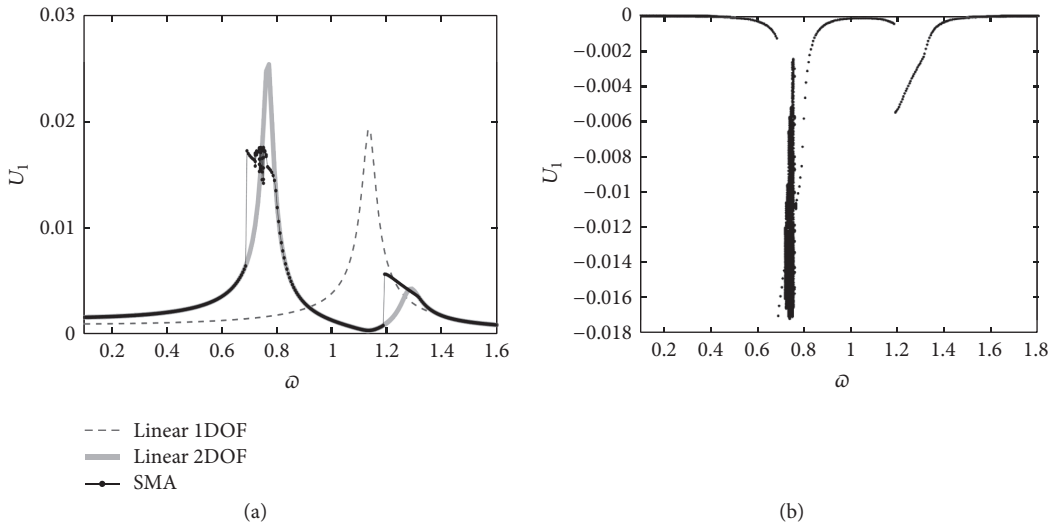


Figure 5: Primary system response with $\delta = 0.0011$ and $\gamma_m = 0.15$ in down-sweep test: (a) maximum amplitude; (b) bifurcation diagram.

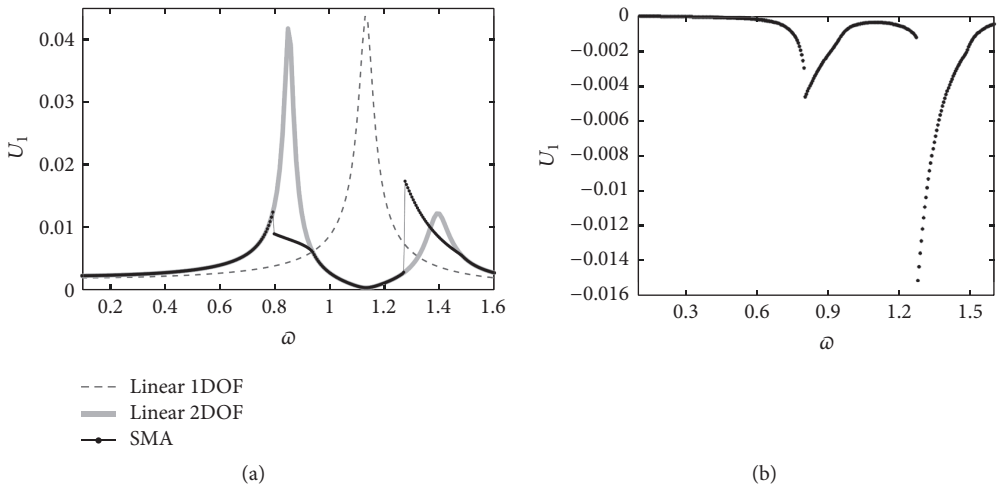


Figure 6: Primary system response in up-sweep test: (a) maximum amplitude; (b) bifurcation diagram.

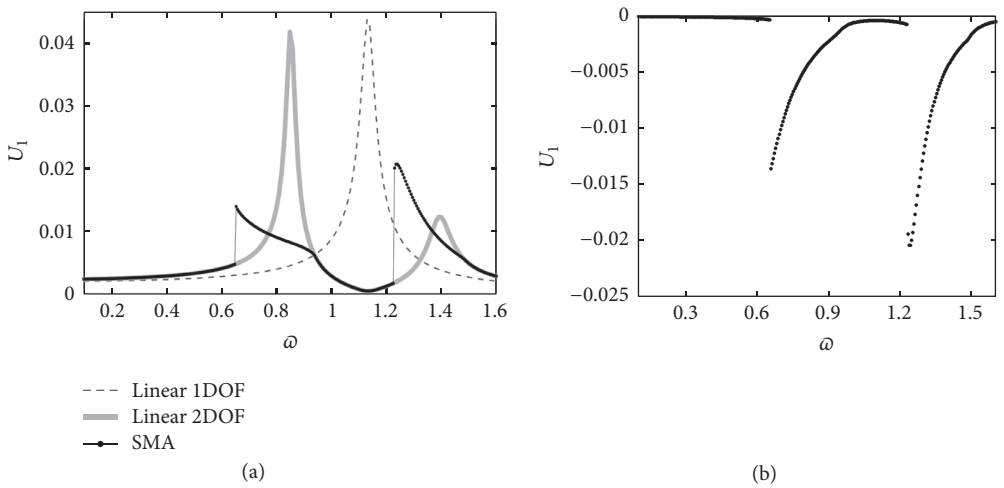


Figure 7: Primary system response with $\delta = 0.0025$ and $\gamma_m = 0.22$ in down-sweep test: (a) maximum amplitude; (b) bifurcation diagram.

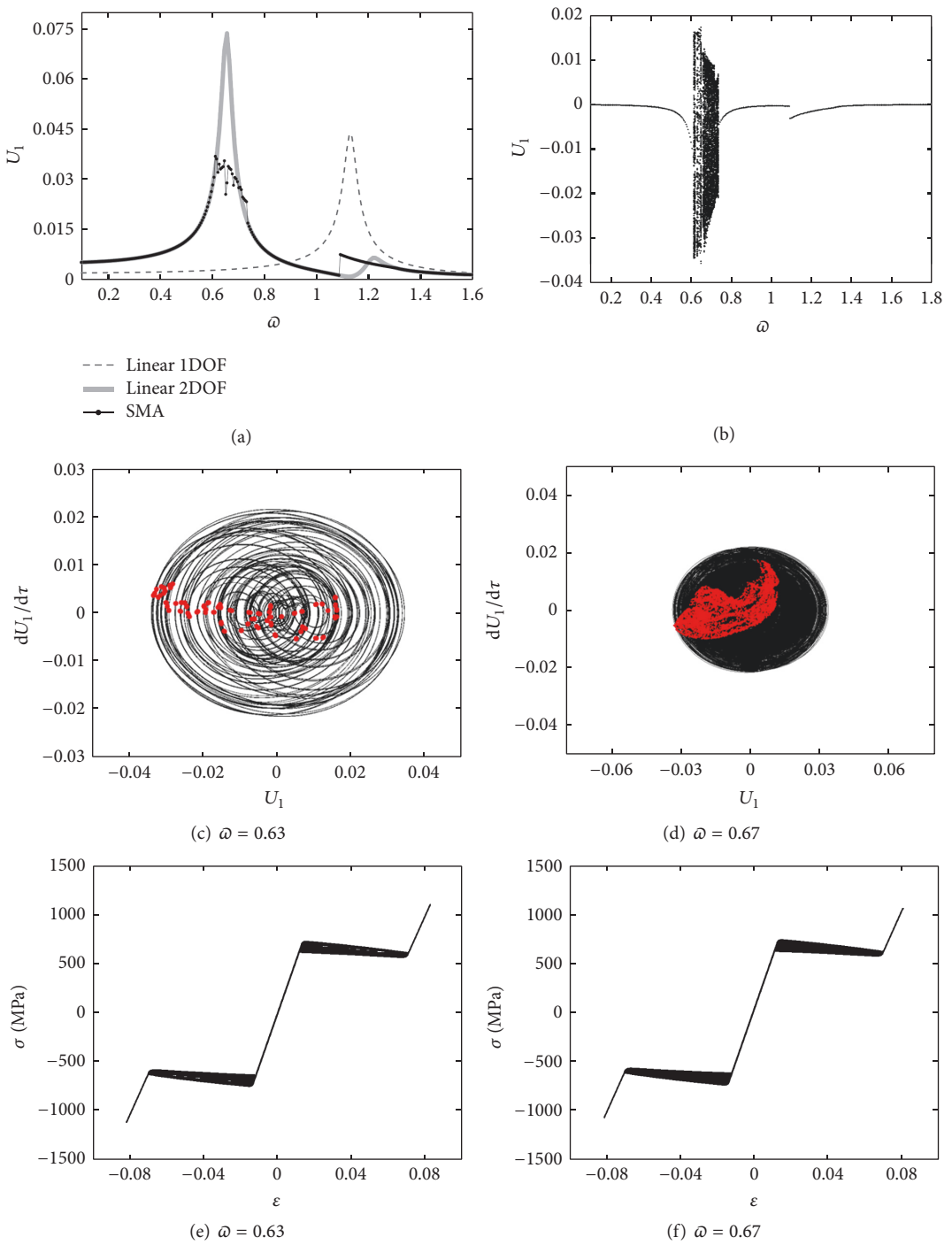


FIGURE 8: Primary system response with $\delta = 0.0025$ and $\gamma_m = 0.1$ in up-sweep test: (a) maximum amplitude; (b) bifurcation diagram; (c-d) phase space with Poincaré section; (e-f) stress-strain curves.

for $\gamma_m < 0.22$, a complex behavior appears in the first resonance region and, depending on the value of forcing amplitudes, $\delta$, and forcing frequency, $\varpi$, quasi-periodic-like pattern or chaotic-like pattern responses are observed. For $\gamma_m < 0.22$, the system presents complex behavior and the maximum amplitude of primary system is generally lower than the response of the classical TVA. When mass ratios increase, $\gamma_m \geq 0.22$, the primary system presents periodic response; however, two resonance peaks appear together with dynamical jumps, and maximum amplitudes are comparable to the TVA system.

It is really interesting that a chaotic-like response can lead to smaller vibration amplitudes than a periodic behavior for the same forcing parameters. This point should be further

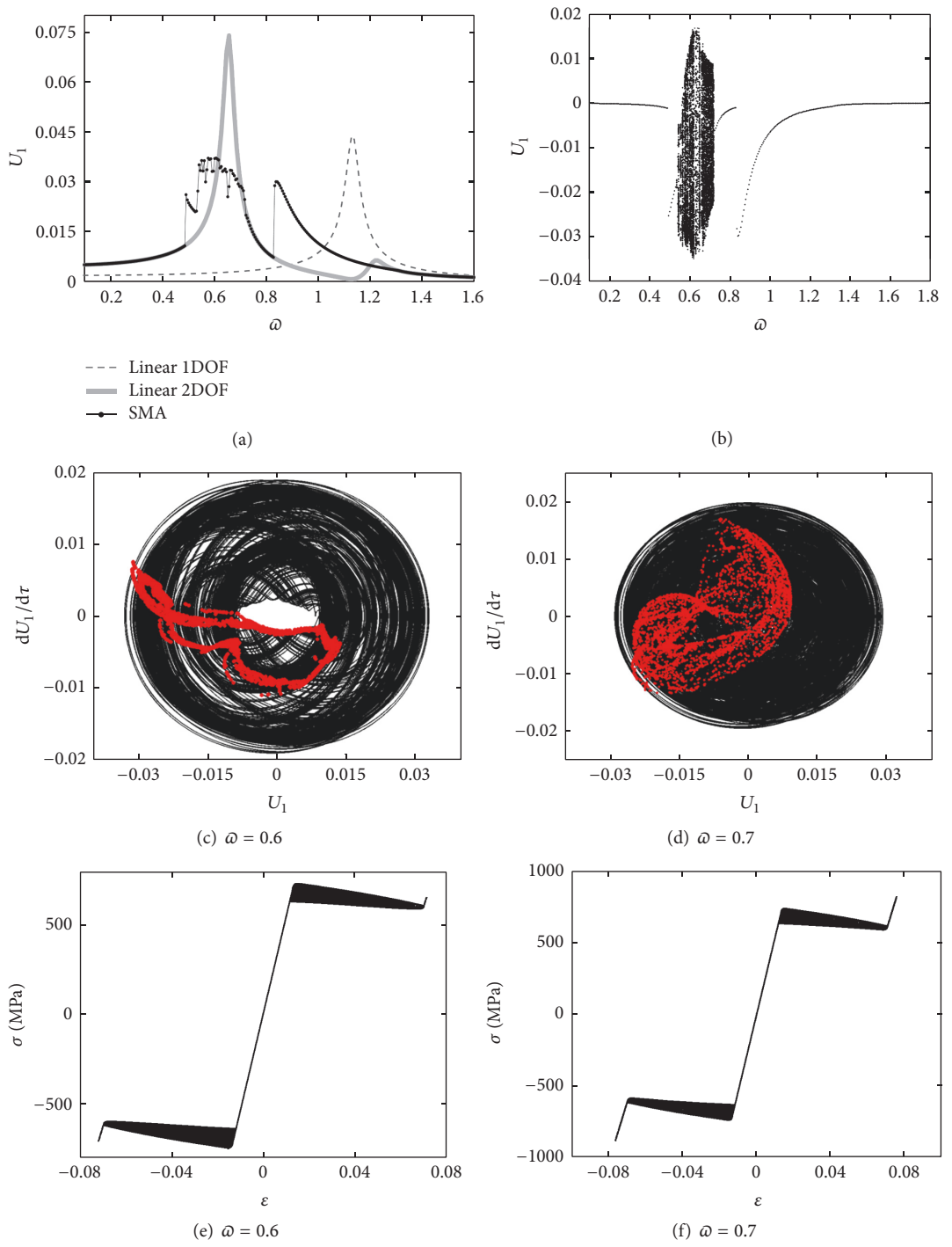


FIGURE 9: Primary system response with $\delta = 0.0025$ and $\gamma_m = 0.1$ in down-seep test: (a) maximum amplitude; (b) bifurcation diagram; (c-d) phase space with Poincaré section; (e-f) stress-strain curves.

investigated in order to evaluate which situation is desirable. Fatigue may be the essential point to establish a design decision defining if it is better to have smaller amplitudes in chaotic regime or higher amplitudes in periodic response.

In order to consider the performance of SMA-ATVA, another important point should be addressed. Tuned frequencies are temperature dependent and, therefore, can be altered. Savi et al. [18] discussed the general aspects of adaptive behavior of ATVA. Aguiar et al. [24] confirmed these conclusions from an experimental point of view.

## 5. Conclusions

This paper deals with the use of SMA elements in vibration absorbers. Dynamical analysis of passive pseudoelastic tuned vibration absorber (ATVA) with an SMA element is carried

out and the behavior trends of this system are compared with a passive absorber with a linear elastic element (TVA). A parametric analysis is carried out from numerical simulations monitoring the maximum amplitude of the primary system. Proper choices of mass ratio and suitable range of forcing amplitude make the SMA-ATVA have a good performance. Stress-induced phase transformations and their hysteretic behavior are the main driving aspects to define absorber performance. Nevertheless, strong nonlinear effects of the adaptive vibration absorber introduce complex dynamical responses that should be properly investigated during the design of such systems. Chaos, quasiperiodicity, and dynamical jumps are some aspects that need to be evaluated. An essential point that needs to be highlighted is the adaptive characteristic of the SMA absorbers making possible that tuned frequency can be altered by temperature changes, increasing the advantages of this kind of system.

## Conflicts of Interest

The authors declare that there are no conflicts of interest regarding the publication of this paper.

## Acknowledgments

The authors acknowledge the support of the Brazilian Research Agencies CNPq, CAPES, and FAPERJ. The Air Force Office of Scientific Research (AFOSR) is also acknowledged.

## References

[1] D. J. Inman, *Vibration with Control, Measurement and Stability*, Prentice Hall, Upper Saddle River, NJ, USA, 1989.

[2] R. A. Ibrahim, "Recent advances in nonlinear passive vibration isolators," *Journal of Sound and Vibration*, vol. 314, no. 3–5, pp. 371–452, 2008.

[3] M. J. Brennan, "Some recent developments in adaptive tuned vibration absorbers/neutralisers," *Shock and Vibration*, vol. 13, no. 4-5, pp. 531–543, 2006.

[4] M. A. Savi, "Nonlinear dynamics and chaos in shape memory alloy systems," *International Journal of Non-Linear Mechanics*, vol. 70, pp. 2–19, 2015.

[5] M. A. Savi and P. M. C. L. Pacheco, "Chaos and hyperchaos in shape memory systems," *International Journal of Bifurcation and Chaos*, vol. 12, no. 3, pp. 645–657, 2002.

[6] L. G. Machado, M. A. Savi, and P. M. C. L. Pacheco, "Nonlinear dynamics and chaos in coupled shape memory oscillators," *International Journal of Solids and Structures*, vol. 40, no. 19, pp. 5139–5156, 2003.

[7] D. Bernardini and G. Rega, "Thermomechanical modelling, nonlinear dynamics and chaos in shape memory oscillators," *Mathematical and Computer Modelling of Dynamical Systems*, vol. 11, no. 3, pp. 291–314, 2005.

[8] M. A. Savi, M. A. N. Sá, A. Paiva, and P. M. C. L. Pacheco, "Tensile-compressive asymmetry influence on shape memory alloy system dynamics," *Chaos, Solitons and Fractals*, vol. 36, no. 4, pp. 828–842, 2008.

[9] H. S. Oliveira, A. S. De Paula, and M. A. Savi, "Dynamical jumps in a shape memory alloy oscillator," *Shock & Vibration*, vol. 2014, article 656212, Article ID 656212, 2014.

[10] E. Sitnikova, E. Pavlovskaia, M. Wiercigroch, and M. A. Savi, "Vibration reduction of the impact system by an SMA restraint: numerical studies," *International Journal of Non-linear Mechanics*, vol. 45, no. 9, pp. 837–849, 2010.

[11] B. C. dos Santos and M. A. Savi, "Nonlinear dynamics of a nonsmooth shape memory alloy oscillator," *Chaos, Solitons and Fractals*, vol. 40, no. 1, pp. 197–209, 2009.

[12] D. C. Lagoudas, M. M. Khan, J. J. Mayes, and B. K. Henderson, "Pseudoelastic SMA spring elements for passive vibration isolation: part II - simulations and experimental correlations," *Journal of Intelligent Material Systems and Structures*, vol. 15, no. 6, pp. 443–470, 2004.

[13] S. Saadat, J. Salichs, M. Noori et al., "An overview of vibration and seismic applications of NiTi shape memory alloy," *Smart Materials and Structures*, vol. 11, no. 2, pp. 218–229, 2002.

[14] M. H. Elahinia, J.-H. Koo, and H. Tan, "Improving robustness of tuned vibration absorbers using shape memory alloys," *Shock and Vibration*, vol. 12, no. 5, pp. 349–361, 2005.

[15] K. Williams, G. Chiu, and R. Bernhard, "Adaptive-passive absorvers using shape-memory alloys," *Journal of Sound and Vibration*, vol. 249, no. 5, pp. 835–848, 2002.

[16] K. A. Williams, G. T.-C. Chiu, and R. J. Bernhard, "Dynamic modelling of a shape memory alloy adaptive tuned vibration absorber," *Journal of Sound and Vibration*, vol. 280, no. 1-2, pp. 211–234, 2005.

[17] E. Rustighi, M. J. Brennan, and B. R. Mace, "A shape memory alloy adaptive tuned vibration absorber: design and implementation," *Smart Materials and Structures*, vol. 14, no. 1, pp. 19–28, 2005.

[18] M. A. Savi, A. S. de Paula, and D. C. Lagoudas, "Numerical investigation of an adaptive vibration absorber using shape memory alloys," *Journal of Intelligent Material Systems and Structures*, vol. 22, no. 1, pp. 67–80, 2011.

[19] D. C. Lagoudas, *Shape Memory Alloys: Modeling and Engineering Applications*, Springer, New York, NY, USA, 2008.

[20] A. Paiva and M. A. Savi, "An overview of constitutive models for shape memory alloys," *Mathematical Problems in Engineering*, vol. 2006, Article ID 56876, pp. 1–30, 2006.

[21] A. Paiva, M. A. Savi, A. M. B. Braga, and P. M. C. L. Pacheco, "A constitutive model for shape memory alloys considering tensile-compressive asymmetry and plasticity," *International Journal of Solids and Structures*, vol. 42, no. 11-12, pp. 3439–3457, 2005.

[22] H. S. Oliveira, *Analysis of A Pseudoelastic Vibration Dynamical Absorber [M.Sc. Thesis]*, University of Brasilia, Brasília, Brazil, 2014, http://repositorio.unb.br/handle/10482/16290.

[23] M. Ortiz, P. M. Pinsky, and R. L. Taylor, "Operator split methods for the numerical solution of the elastoplastic dynamic problem," *Computer Methods in Applied Mechanics and Engineering*, vol. 39, no. 2, pp. 137–157, 1983.

[24] R. A. A. Aguiar, M. A. Savi, and P. M. C. L. Pacheco, "Experimental investigation of vibration reduction using shape memory alloys," *Journal of Intelligent Material Systems and Structures*, vol. 24, no. 2, pp. 247–261, 2013.